# A novel IL/MOF nanocomposite tailored for trace SO2 efficient capture based on synergistic effects

Huifang Zhao[1], Xingping Gu[1], Guopeng Han[2], and Dahuan Liu[1]

[1]Beijing University of Chemical Technology
[2]Heze University

August 13, 2022

**Abstract**

Due to its toxicity and corrosiveness, it is of enormous significance to efficiently capture and recover sulfur dioxide (SO2) from flue gas and natural gas. Herein, a new type of IL/MIL-0.7 composite was precisely designed to meet this challenge, which exhibits a high adsorption capacity for SO2 (13.17 mmol·g-1) at 298 K and 1 bar while excludes almost completely carbon dioxide (CO2) (0.27 mmol·g-1) and nitrogen (N2) (0.07 mmol·g-1). The high IAST selectivity (at least 11925) of IL/MIL-0.7 for SO2/CO2 can be achieved within the whole test pressure range. In addition, the breakthrough experiment also confirmed the excellent performance of the composite for deep removal of 2000 ppm SO2. Furthermore, the IL/MIL-0.7 composites can maintain excellent performance after four adsorption and desorption circulations and the thermostability can up to ~450 K. Therefore, this stable IL@MOF composite has the potential application as an effective adsorbent for SO2 removal from flue gas.

## A novel IL/MOF nanocomposite tailored for trace $SO_2$efficient capture based on synergistic effects

*Huifang Zhao[a,++], Xingping Gu[a,++], Guopeng Han[b,*], Dahuan Liu[ac,*]*

[a] State Key Laboratory of Organic-Inorganic Composites, Beijing University of Chemical Technology, North Third Ring Road 15, Chaoyang District, Beijing 100029, P. R. China

[b] Department of Chemistry and Chemical Engineering, Heze University, Heze 274000, P. R. China

[c] College of Chemical Engineering, Qinghai University, Xining 810016, P. R. China

**E-mails: hanguopeng@hezeu.edu.cn (G.H.);*

*Dahuan_ Liu@outlook.com (D.L.).*

*[++] These authors contributed equally.*

**Abstract**

Due to its toxicity and corrosiveness, it is of enormous significance to efficiently capture and recover sulfur dioxide ($SO_2$) from flue gas and natural gas. Herein, a new type of IL/MIL-0.7 composite was precisely designed to meet this challenge, which exhibits a high adsorption capacity for $SO_2$ (13.17 mmol·g$^{-1}$) at 298 K and 1 bar while excludes almost completely carbon dioxide ($CO_2$) (0.27 mmol·g$^{-1}$) and nitrogen ($N_2$) (0.07 mmol·g$^{-1}$). The high IAST selectivity (at least 11925) of IL/MIL-0.7 for $SO_2/CO_2$ can be achieved within the whole test pressure range. In addition, the breakthrough experiment also confirmed the excellent performance of the composite for deep removal of 2000 ppm $SO_2$. Furthermore, the IL/MIL-0.7 composites can maintain excellent performance after four adsorption and desorption circulations and the thermostability

can up to ~450 K. Therefore, this stable IL/MOF composite has the potential application as an effective adsorbent for $SO_2$removal from flue gas and natural gas.

**Keywords:** ionic liquids, metal-organic frameworks, molecular-sieving separation, $SO_2$ capture

## 1. Introduction

Combustion of fossil fuels, including coal, oil, and natural gas, produces sulfur dioxide ($SO_2$), which is an irritant, corrosive, and highly toxic gas [1-5]. With the growth of the world economy, the emission of $SO_2$ has increased significantly to meet the increasing energy demand [6]. However, even trace $SO_2$ (*e.g.* 1000–3000 ppm) can cause severe environmental problems (*e.g.* smog and acid rain). Besides, it can irritate the lungs and induce cancer once $SO_2$ enters the respiratory tract of humans[7]. Therefore, the effective removal of $SO_2$ from the air has become an essential issue to ensure human health and environmental safety. At present, various desulfurization technologies have been developed to remove $SO_2$ from flue gas and natural gas, such as washing with limestone slurry, ammonia and liquid adsorbents [8]. However, these technologies are accompanied by great challenges, for example, low $SO_2$ capture efficiency, high operation cost, corroding pipelines and producing large numbers of secondary pollutants [9-11]. Although dry adsorption technologies based on porous materials (including zeolite, activated carbon, and metal oxides) can avoid solvent consumption, they have low adsorption capacity, high energy consumption for regeneration, and poor durability[12-13]. In addition, trace $SO_2$ will permanently deactivate amines and reduce the efficacy of the $CO_2$ scrubbing process. Extremely poor absorption and low selectivity of $SO_2$ relative to $N_2$ and $CO_2$ make the complete removal of trace $SO_2$ a formidable issue [14,15]. Thus, designing a new porous adsorbent to efficiently capture $SO_2$ from flue gas and natural gas with high selectivity to achieve sustainable development.

Metal-organic frameworks (MOFs), with large specific surface area, high designability and tunability, have attracted extensive attention in $SO_2$ adsorption and separation [14]. Nevertheless, the causticity of $SO_2$ may damage the coordination bonds between metal clusters and organic ligands in MOFs[6]. For example, Janiak et al. suggested that MOF-177 (BET = 4100 $m^2 \cdot g^{-1}$) has an ultra-high $SO_2$ adsorption capacity (25.7 $mmol \cdot g^{-1}$at 298 K and 1 bar). However, the formation of metal-sulfur bonds disrupted the coordination bonds in MOFs which further induces its structure to collapse [16]. At present, some highly stable MOFs with high adsorption capacity for $SO_2$ have been reported, such as DUT-67(Zr) (9 $mmol \cdot g^{-1}$) and Zr-Fum (4.9 $mmol \cdot g^{-1}$) [17]. Unfortunately, these stable MOFs also suffered the low adsorption capacity of $SO_2$ [6]. It should be noted that $SO_2$ is often combined with several competitive gases such as $CO_2$ and $N_2$ [11]. However, only a few MOFs can selectively capture $SO_2$from $CO_2$ and $N_2$, especially in the case of deep desulfurization [16,18]. For instance, Bao et al. revealed the Mg-gallate showed a high IAST selectivity of 325 for $SO_2/CO_2$ mix-gases [14]. Xing and co-workers reported that the adsorption capacity of SIFSIX-2-Cu-i for $SO_2$ can arrive at 6.9 $mmol \cdot g^{-1}$ and the selectivity of $SO_2/CO_2$ is 87 [19]. MFM-601 displayed a high $SO_2$ capacity (12.3 $mmol \cdot g^{-1}$) at 298 K and 1 bar, while the selectivities for $SO_2/CO_2$ and $SO_2/N_2$ only reach 32 and 255[20]. Therefore, from a practical perspective, it is essential to design a series of new adsorbents with high adsorption capacity and high stability for $SO_2$, and virtually exclude $CO_2$ and $N_2$ adsorption. Recently, ionic liquids (ILs) have been widely applied in $SO_2$adsorption studies due to their unique physicochemical properties, including low vapor pressure, high stability, and tunability[21]. Unfortunately, the high viscosity of ILs can cause poor mass transfer and hamper their industrial application. To overcome the difficulties, silica gel, porous carbon and silica have been used as supports to disperse IL and change the adsorption capacity of $SO_2$ [22]. Compared with these materials, MOFs with large surface area and tunable size have been used as outstanding porous supports for the incorporation of ILs. More importantly, the introduction of IL may provide additional adsorption sites to enhance gas adsorption and separation performance of adsorbent[23]. For example, IL/MOF composites have been extensively investigated on $NH_3$, $CO_2$,and $H_2O$ in our research group, exhibiting excellent adsorption performances [24-26].

Herein, a novel composite material IL/MIL was designed and synthesized, as shown in Scheme 1. The introduction of IL endows the adsorbent with unique adsorption sites (-OH, -Cl and the long alkyl chain in IL) for $SO_2$. Besides, the composite of IL/MIL can provide adequate space to effectively capture $SO_2$, such as the free space originating from the alkyl chain in IL and the inner surface of composites. Then, the

experiment indicated that IL/MIL-0.7 showed a high $SO_2$ adsorption capacity (13.18 mmol·g$^{-1}$) at 298 K and 1 bar, almost totally excluding $CO_2$ (0.27 mmol·g$^{-1}$) and $N_2$ (0.07 mmol·g$^{-1}$). Also, for the mixture of 10% $SO_2$ and 90% $CO_2$, the $SO_2/CO_2$ selectivity could reach to11925 while the sorbent selection parameter ($S_{sp}$) could be as high as 472131, both of which are higher than those reported porous materials. In addition, the excellent performance of the composite for the deep removal of 2000 ppm $SO_2$ also was confirmed by breakthrough experiments with the $SO_2/N_2/CO_2$ mixed gas. These reveal that the IL/MIL-0.7 composite has the potential application to remove $SO_2$ efficiently from flue gas and natural gas.

## 2. Materials and experiments

### 2.1. Materials

chromium (III) nitrate nonahydrate ($Cr(NO_3)_3{\cdot}9H_2O$) and 1,4-ben-zenedicarboxylic acid ($H_2BDC$) were obtained from J&K (China). N-methylimidazolium and chlorobutanol were purchased from Shanghai Bide Pharmatech Ltd. *N,N* -dimethylforma-mide (DMF), methanol and ethyl acetate were obtained from Beijing Chemical Works. All chemicals were utilized directly from commercial purchases and without additional purification.

### 2.2. Preparation of materials

According to reported work[27], MIL-101(Cr) was prepared by $H_2BDC$ and $Cr(NO_3)_3{\cdot}9H_2O$.

**IL/MIL-x** : MIL-101(Cr) was degassed by vacuum activation at 353 K before sample preparation. Then, a methanol solution of [BOHmim]Cl was mixed with activated MIL-101(Cr) powder, and the mixture was magnetically agitated at 298 K for 1 h. Subsequently, the sample was dried at 378 K for 12 h in an oven. The composites are identified as IL/MIL-x, where x is the weight percentage of IL in the composite (for example, x = 0.2, 0.4, 0.7).

Detailed procedures for synthesizing [BOHmim]Cl, MIL-101(Cr) and IL/MIL-x are shown in Section S1 of Supporting Information (SI).

### 2.3. Characterizations

An X-ray diffractometer (D8 ADVANCE) from Bruker (Germany) was used to perform powder X-ray diffraction (PXRD) throughout the 2 range of 5-40° with a scan speed of 5° min$^{-1}$ and a step size of 0.02deg. The Brunauer-Emmett-Teller (BET) surface area and pore volume of material were determined with a gas adsorption analyzer (Best, China). Fourier transform infrared (FT-IR) was carried out with a Thermo Scientific Nicolet iS5 spectrophotometer. The spectra data were measured from 4000 to 400 cm$^{-1}$. For the analysis of solid samples, the samples were mixed with pure potassium bromide (KBr) and sample (about 1:100 mass ratio), the sample powder was compressed into flakes with a tablet machine, and then tested in an infrared instrument. Pure ILs samples were firstly pressed to be tablets with dry pure potassium bromide, then applied on potassium bromide by a small amount of IL and put on the instrument for testing. The morphologies of samples were investigated with scanning electron microscopy (SEM, Gemini SEM 300). Energy dispersive spectroscopy (EDS) elemental mapping images were performed. Transmission electron microscope (TEM) images were measured by a Japan-JEOL-JEM 2011Plus. X-ray photoelectron spectroscopy (XPS) was attained on a Thermo Scientific K-Alpha with Al Kα radiation. Thermogravimetric analysis (TGA) data were recorded using Japan-Hitachi-TG DTA7200. Instrument under $N_2$ atmosphere with a heating rate of 10 K·min$^{-1}$ from 298 K to 783 K.

### 2.4. Adsorption measurements

The adsorption isotherms of $SO_2$ by IL/MILs were determined on the BSD-PM analyzer. Before each adsorption experiment, around 100 mg of samples were weighed and degassed at 353 K and vacuum (<$10^{-5}$ Pa) for 12 h. Furthermore, the adsorption isotherms of $CO_2$ and $N_2$ at 298 K by IL/MILs were determined on BSD-PS (M) analyzer and ASAP 2020 plus HD88 physisorption analyzer (Micromeritics, USA), respectively.

### 2.5 Breakthrough experiment

The breakthrough experiment for the removal of 2000 ppm $SO_2$ was performed at 298 K and 1 bar (Figure S1). In the dynamic separation experiment, the stainless-steel column with an inner diameter of 11 millimeters and a loading length of 59 mm was filled with 1.0582 grams of IL/MIL. The activation of samples was carried out with a carrier gas (He [?] 99.999%, 30 mL*min$^{-1}$) purged for 2 h at 373 K. Then, the mixed gas consisting of 2000 ppm $SO_2$, 15% $CO_2$ and 84.8% $N_2$ was pumped at the rate of 40 mL*min$^{-1}$ for the adsorption of $SO_2$. The mass spectrometer (MS) continuously monitored the recovered gas passed through the adsorption bed.

## 3. Results and discussion

### 3.1 Characterization

PXRD patterns of MIL-101(Cr) and IL/MIL-x were carried out. Figure 1a indicates that the PXRD patterns of MIL-101(Cr) correspond well with their simulated ones, confirming the successful synthesis[28]. Besides, the IL/MIL composites maintain similar diffraction peaks to pristine MIL-101, indicating that the materials retain the framework stability after loading IL. However, the characteristic peaks of IL/MIL at 5-7deg are weakened, which may be ascribed to an alteration in electron density, morphology, as well as crystallization [29-31]. Then, the porosity of the adsorbents was evaluated by analyzing the $N_2$adsorption/desorption isotherms at 77 K. Figures 1b and 1c suggest that the $N_2$ uptake and the pore size of samples gradually decrease with increasing the content of loaded IL. As listed in Table S1, the BET surface area of the sample decreases from 3111 $m^2*g^{-1}$ to 3 $m^2*g^{-1}$ and the total pore volume decreased from 2.0 $cm*g^{-1}$ to 0.14 $cm^3*g^{-1}$ with the increase of IL content, which can be ascribed to the pore blockage resulted by the IL entering the pore of MIL-101(Cr). Furthermore, FT-IR spectra of MIL-101(Cr) and IL/MIL-x are shown in Figure 1d. The asymmetric and symmetric stretching vibrations of the dicarboxylate linker O–C–O can be observed at 1624 and 1401 cm$^{-1}$[32]. In addition, other bands on the benzene ring of the ligand can be found at 1507 cm$^{-1}$ (C=C stretching) and 1158, 1107, 882 and 748 cm$^{-1}$ (C-H bending)[31,33]. These demonstrate the MOF framework is well preserved after loading IL, indicating that the loaded IL does not affect the structural integrity. Besides, new peaks were observed in IL/MIL composites. For instance, the peak situated at 1579 cm$^{-1}$ and the weak peaks at 2951 and 2852 cm$^{-1}$ can be ascribed to the stretching vibration of C-N [31,34] and the C-H stretching vibration of the alkyl chain in IL[32,35]. The above evidence indicates that IL is successfully loaded in MIL-101(Cr).

To further illustrate the existence of IL, the XPS spectra and EDS mapping were investigated by using IL/MIL-0.7 as a case study. Compared with that of MIL-101(Cr) (Figure 2), the spectrum of IL/MIL-0.7 displays the characteristic peaks corresponding to Cl and N elements. EDS mapping under SEM mode of IL/MIL-0.7 shows the homogeneous distribution of N and Cl elements (Figures S2c and S2d), which shows the excellent dispersion performance of IL in MIL-101(Cr). SEM images further confirmed the maintenance of crystal morphology. IL/MIL-0.7 has similar particle sizes (200–500 nm) and octahedral crystals typical of MIL-101(Cr) as shown in Figures S2a and 2b. Additionally, TEM analysis (Figure 3) reveals a layer of transparent substance with a non-uniform thickness (more than 15 nm) on the outside of IL/MIL-0.7 compared with pristine MIL-101(Cr), suggesting that IL was deposited on the outer surface of MIL-101(Cr). The above characterization data demonstrate the successful loading of IL.

### 3.2 $SO_2$adsorption performance

To evaluate the properties of the composites, the adsorption isotherms of $SO_2$ over four adsorbents were determined by the volumetric method at 298 K and 1 bar. Figure 4a indicates that the maximum adsorption uptake of IL/MIL-x decreases compared with MIL-101(Cr) due to the reduction of pore volume and the different adsorption sites caused by the introduction of IL [9,19]. Besides, the saturated adsorption capacity of $SO_2$ changes with the increase of loaded IL content. As shown in Figure 4a and Table S2, the $SO_2$ uptake capacity of IL/MIL-0.7 and IL/MIL-0.4 is (13.18 and 11.36 mmol*g$^{-1}$, respectively) lower than that of IL/MIL-0.2 (13.51 mmol*g$^{-1}$) at 298 K and 1 bar. Due to the BET surface area of the composite decreasing with the increasing IL content, the adsorption capacity of the porous carrier drops somewhat. Interestingly, the $SO_2$ adsorption capacity of IL/MIL-0.7 (13.18 mmol*g$^{-1}$) is higher than IL/MIL-0.4 (11.36 mmol*g$^{-1}$),

but the BET and pore volume of the former material is smaller than those of the latter. This indicates that the introduction of IL induces additional adsorption sites for the adsorbent, prompting the capture of $SO_2$. Therefore, it can be concluded that the saturated adsorption capacity is not only determined by the specific surface area and pore volume but also depends on the action of IL. Although the adsorption capacity of IL/MIL-0.7 is subequal to that of MIL-101(Cr) at 298 K and 1 bar, its performance is better than some other materials previously reported, including PI-COF-m10 (6.3 mmol*$g^{-1}$) [36], and other typical porous materials, such as SIFSIX-1-Cu (11.01 mmol*$g^{-1}$)[19], Ph-4MVIm-Br (8.12 mmol*$g^{-1}$)[18], MFM-300(In) (8.28 mmol*$g^{-1}$)[15], MIL-160 (7.2 mmol*$g^{-1}$)[16], ECUT-111(11.6 mmol*$g^{-1}$)[37], SIFSIX-2-Cu-I (6.90 mmol*$g^{-1}$) [20], SIFIX-3-Ni (4.30 mmol*$g^{-1}$) [19], CPL-1 (1.999 mmol*$g^{-1}$) [38], ELM-12 (2.73 mmol*$g^{-1}$) [39], NPC-1 (2.45 mmol*$g^{-1}$) [40], and MFM-601 (12.3 mmol*$g^{-1}$) [20] (Table S2). Notably, the low-pressure adsorption capacity is increased for IL/MIL with the increase of the loaded IL content, as shown in Figure 4b. The $SO_2$ adsorption capacity of IL/MIL-0.7 significantly exceeds that of pristine MIL-101(Cr) at low partial pressures (below 0.1 bar). Moreover, the $SO_2$ uptake of IL/MIL-0.7 (0.67 mmol*$g^{-1}$) at 0.002 bar exceeds that of MFM-300(In) (0.43 mmol*$g^{-1}$) [15] and MFM-601 (0.24 mmol*$g^{-1}$) [20], only lower than [TMEDA][DES]@BN (0.82 mmol*$g^{-1}$, 293 K) [41], and P(Ph-4MVIm-Br) (1.55 mmol*$g^{-1}$) [18]. However, these two kinds of materials exhibit lower adsorption capacity compared to IL/MIL-0.7 at 1 bar. $SO_2$ adsorption performance is up to 1.68 mmol*$g^{-1}$ when the partial pressure reaches to 0.01 bar, which is more than 3.3 times as high as MIL-101(Cr) (0.5 mmol*$g^{-1}$). As the pressure further increases to 0.1 bar, the adsorption amount of $SO_2$ is up to 4.7 mmol*$g^{-1}$. Compared with the other reported porous materials, this material has a much higher low-pressure adsorption capability, including P(Ph-4MVIm-Br) (4.14 mmol*$g^{-1}$) [18], SIFSIX-2-Cu-i (4.16mmol*$g^{-1}$) [19], and HNIP-TBMB-1(3.54 mmol*$g^{-1}$) [42]. These suggest that IL/MIL-0.7 can provide excellent $SO_2$capacity from low pressures to atmospheric pressures, which is of great importance from a practical point of view.

### 3.3 $SO_2$ separationperformance

Since $SO_2$ is usually involved in many industrial gases as a contaminant, for example, in flue gases ($CO_2$ and $N_2$)[43], it is crucial to explore the separation performance of $SO_2$from gas mixtures. The $CO_2$ and $N_2$adsorption isotherms of IL/MIL-0.7 at 298 K were obtained to evaluate the separation selectivity. Although both $CO_2$ and $SO_2$ are acid gases, their adsorption isotherms on the composites have different adsorption behaviors. As shown in Figure 5a, the adsorption capacity of $SO_2$ (13.18 mmol*$g^{-1}$) was significantly higher than that of $CO_2$ (0.27 mmol*$g^{-1}$) and $N_2$ (0.07 mmol*$g^{-1}$) in IL/MIL-0.7. This variation in the adsorption capacity can be attributed to the introduction of IL which induces unique adsorption sites for $SO_2$. In detail, the strong adsorption interaction between $SO_2$ and IL/MIL-0.7 pushes the $SO_2$ to overcome the large mass transfer resistance of the IL layer to enter the material, while $CO_2$ and $N_2$ cannot penetrate the adsorbent due to their weak force between them. Therefore, IL/MIL-0.7 exhibits larger $SO_2$ capacity and lower $N_2$ and $CO_2$ uptake. Furthermore, from the comparison of the $SO_2$ adsorption capacity of IL/MIL-0.7 with reported porous materials in Figure 5b and Table S2, IL/MIL-0.7 shows superior $SO_2$ adsorption capacity. More importantly, the $CO_2$ and $N_2$ uptakes of IL/MIL-0.7 are significantly lower than other adsorbents reported.

To further evaluate the separation efficiency, $SO_2/CO_2$ selectivity was calculated based on the ideal adsorption solution theory (IAST) (Section 2 in SI). Firstly, the dual-site Langmuir (DSL) model was used to fit the adsorption isotherm (eq. S1), and then the separation selectivity was calculated by eq. S2 from the single-component gas adsorption isotherms. Fitted curves and fitted parameters can be found in Figure S3 and Table S2, respectively. As expected, the composite exhibits an ultra-high $SO_2/CO_2$selectivity over $10^4$ (about 11925) for a mixture of 10% $SO_2$ and 90% $CO_2$ at 298 K and 1.0 bar (Figure 6a). The excellent adsorption selectivity towards $SO_2$ for IL/MIL-0.7 can be explained by a molecular-sieve effect. The introduction of IL led to selective permeation, whereas $SO_2$ can be accessible to the interlayer spaces IL/MIL-0.7 while the $CO_2$ and $N_2$molecules are excluded by their weak adsorption interaction. Then, the $S_{SO2/CO2}$ of IL/MIL-0.7 was compared with the reported adsorbent. Figure 6b indicates that the separation performance of IL/MIL-0.7 is significantly higher than those in the benchmark materials (Figure 6b and Table S2), such as Mg-gallate (325) [14], and P([allyl-TMG]Br-DVB)(452) [8]. Furthermore, for a pressure swing adsorption (PSA) process, selectivity and working capacity are typically regarded as two crucial criteria to identify a

new adsorbent, while the sorbent selection parameter ($S_{sp}$), combining selectivity and working capacity in a single parameter, can be used to better evaluate the potential of adsorbent. Therefore, the value of$S_{sp}$ of IL/MIL-0.7 for $SO_2/CO_2$ is calculated by eq. S3 and compared with the value of reported adsorbents. Figure 6c indicates that IL/MIL-0.7 exhibits a higher value of $S_{sp}$ (about 472131) than the majority of other materials. To summarize, IL/MIL-0.7 has a good potential to capture trace $SO_2$ with high selectivity during the flue gas desulfurization (FGD) process.

It is well known that the content of $SO_2$ in industrial flue gas (such as coal combustion flue gas) is very low (about 2000 ppm)[41,44]. To confirm the practical ability of IL/MIL-0.7 to capture trace $SO_2$ and the feasibility of composites in the application process, the breakthrough experiment was carried out on the simulated flue gas at 298 K and 1.0 bar, that is, a ternary gas mixture $SO_2/CO_2/N_2$ (2000 ppm/15%/84.8%, v/v/v) containing 2000 ppm $SO_2$ with a flow rate of 40 mL*min$^{-1}$. Figure 7 indicates that $CO_2$ and $N_2$ rapidly elute through the column at the beginning, while the breakthrough time of $SO_2$ on IL/MIL-0.7 could reach up to 130 min*g$^{-1}$, which means that the material can realize the deep and selective removal of trace $SO_2$. The breakthrough selectivity of $SO_2/CO_2$ in such ternary gas mixture $SO_2/CO_2/N_2$ can reach up to 668 calculated by eq. S4, which is at least 5–9 times higher than those in other materials reported in the literature (Figure 7b).

To assess the binding energy between IL/MIL-0.7 and different gas molecules, single-component adsorption isotherms were compared at different temperatures. As shown in Figures 8a and 8b, the adsorption capacity of both decreases significantly with the increase in temperature, indicating an exothermic adsorption process. The heats of adsorption ($Q_{st}$) of $SO_2$ and $CO_2$ were calculated using the Clausius-Clapeyron equation (eq. S5) (Figures 8c and 8d), which is from 20 to 40 kJ*mol$^{-1}$ for $SO_2$ while from 0 to 4 kJ*mol$^{-1}$ for $CO_2$. This indicated that the affinity of IL/MIL-101 for $SO_2$ is strong than that for $CO_2$. To further explore the interaction between $SO_2$ and composites, FT-IR and XPS spectra were used to evaluate possible $SO_2$ adsorption sites in IL/MIL-0.7. Firstly, the IL/MIL-0.7 before and after $SO_2$ absorption was characterized by FT-IR. Figure S4 demonstrates that the intensity of the hydroxyl peaks of IL/MIL-0.7 after adsorbing $SO_2$ is weakened, indicating that $SO_2$ interacts with the hydroxyl groups[45]. No symmetric or asymmetric stretch band (between 1389 cm$^{-1}$ and 1085 cm$^{-1}$) was observed for $SO_2$, probably because of the overlap with the strong vibrational band of IL/MIL-0.7. At the same time, the characteristic peak of the S element appears in the XPS spectrum, demonstrating that $SO_2$ molecules were adsorbed in the composites (Figure S5a). The binding energy of Cl increases with a deviation of 0.14 eV after IL/MIL-0.7 adsorption of $SO_2$(Figure S5b), which suggests that Cl plays a key role in the adsorption of $SO_2$ [4,46,47]. Acidic hydrogens in $[BOHmim]^+$ such as alkyl side chain C-H and 2-CH can also form two hydrogen bonds with $SO_2$: H***O($SO_2$)-S($SO_2$)[7,48,49]. As a result of the synergistic effect of multiple adsorption sites and the inner surface of the composite, IL/MIL-0.7 has a high adsorption capacity for $SO_2$.

### 3.4 Stability and regeneration properties of composites

Considering the strong corrosive nature of $SO_2$, the regenerative prosperities and thermostability of IL/MIL-0.7 were investigated. Firstly, the regeneration property of IL/MIL-0.7 was evaluated. As shown in Figure 9a, 4 cycles of $SO_2$adsorption were performed to test the reversibility of IL/MIL-0.7, which still maintains good adsorption performance for the fourth time at 1 bar. In addition, FT-IR spectroscopy was employed to assess the completion of $SO_2$ desorption. Compared with the fresh composites, the characteristic peaks of FT-IR spectra did not change significantly (Figure 9b) in recycled IL/MIL-0.7, which means that the material can completely desorb $SO_2$. Furthermore, Figure S6 suggests that the structure of IL/MIL-0.7 can maintain stability until 450 K, demonstrating that IL/MIL-0.7 is stable enough for industrial applications [14]. All these results indicate that the composites have good enough reversibility for $SO_2$ adsorption.

## 4. Conclusion

In conclusion, an IL/MOF composite with multiple adsorption sites has been prepared and used as an efficient adsorbent for $SO_2$capture. IL/MIL-0.7 exhibits a high $SO_2$ capacity at 298 K and 1 bar, and an adsorption capacity of 4.7 mmol*g$^{-1}$ at 298 K and 0.1 bar, which is higher than most known adsorbents

in the literature. Meanwhile, IL/MIL-0.7 excludes $N_2$ and shows high $SO_2/CO_2$ selectivity, up to 11925 for the 10/99 mixture at 298 K and 1 bar. Finally, $SO_2$, $CO_2$ and $N_2$ molecular sieving can be achieved. In addition, the breakthrough experiment of $SO_2/CO_2/N_2$ further proves that IL/MIL-0.7 has excellent trace $SO_2$ capture capacity in its practical application. IL/MOF also exhibits good structural stability and sufficient reversibility. Therefore, loading ILs on MOFs to synthesize new adsorbents shows great potential for a practical flue gas desulfurization process.

**Associated content**

**Supporting Information** :

Preparation of materials, IAST calculations of adsorption selectivity, sorbent selection parameter ($S_{sp}$), breakthrough selectivity, isosteric heat of adsorption, BET specific surface area and pore volume of the material, breakthrough experiments apparatus, SEM and EDS images, comparisons of $SO_2$ uptake and IAST selectivities of $SO_2/CO_2$ of different materials, summaries of the fitted parameter values of the DSL for $SO_2$ and $CO_2$ of IL/MIL-0.7 at 298 K, DSL model of adsorbed data of $SO_2$ and $CO_2$ of IL/MIL-0.7 at 298 K, FT-IR spectra, XPS survey spectra, TGA curve of IL/MIL-0.7.

**Conflict of Interest:**

The authors declare that they have no known competing financial interests or personal relationships that could have appeared to influence the work reported in this paper.

Author information

Corresponding Author

*E-mail: *hanguopeng@hezeu.edu.cn (G.H.);*

*Dahuan_Liu@outlook.com (D.L.).*

**Acknowledgment**

This work was financially supported by the National Key R&D Program of China (2021YFB3802200) and National Natural Science Foundation of China (No. 21978005).

**Reference**

1. Martinez-Ahumada E, Lopez-Olvera A, Jancik V, Sanchez-Bautista JE, Gonzalez-Zamora E, Martis V, Williams DR, Ibarra IA. MOF materials for the capture of highly toxic $H_2S$ and $SO_2$. Organometallics 2020; 39: 883-915.
2. Zhu Q, Li F, Zheng Y, Cao Y, Xiao Y, Liang S, Liu F, Jiang L. Dual-template approach to designing nitrogen functionalized, hierarchical porous carbons for efficiently selective capture and separation of $SO_2$. Sep. Purif. Technol. 2022; 284: 120272-120281.
3. Xing S, Liang J, Brandt P, Schafer F, Nuhnen A, Heinen T, Boldog I, Mollmer J, Lange M, Weingart O. Capture and separation of $SO_2$ traces in metal–organic frameworks via pre-synthetic pore environment tailoring by methyl groups. Angew. Chem. Int. Ed. 2021; 60: 17998-18005.
4. Zhu R, Li G, Lei Z, Gui C. Mechanistic insight into absorption performance assessment for $SO_2$ by mixed ionic liquids. J. Mol. Liq. 2021; 344: 117927-117935.
5. Martinez-Ahumada E, Diaz-Ramirez ML, Lara-Garcia HA, Williams DR, Martis V, Jancik V, Lima E, Ibarra IA. High and reversible $SO_2$ capture by a chemically stable Cr(iii)-based MOF. J. Mater. Chem. A 2020; 8: 11515-11520.
6. Ren Y-B, Xu H-Y, Gang S-Q, Gao Y-J, Jing X, Du J-L. An ultra-stable Zr (IV)-MOF for highly efficient capture of $SO_2$ from $SO_2/CO_2$ and $SO_2/CH_4$ mixtures. Chem. Eng. J. 2022; 431: 134057-134064.
7. Wang L, Zhang Y, Liu Y, Xie H, Xu Y, Wei J. $SO_2$absorption in pure ionic liquids: Solubility and functionalization. J. Hazard. Mater. 2020; 392: 122504-122521.

8. Liu X, Mao F-F, Li Z-M, Xu Z-H, Shu X-J, Mi J-P, Zhou Y, Tao D-J. Solidothermal synthesis of nitrogen-decorated, ordered mesoporous carbons with large surface areas for efficient selective capture and separation of $SO_2$. Chem. Eng. J. 2022; 431: 134142-113131.
9. Zhang L, Xiao L, Zhang Y, France LJ, Yu Y, Long J, Guo D, Li X. Synthesis of ionic liquid-SBA-15 composite materials and their application for $SO_2$ capture from flue gas. Energy Fuels 2018; 32: 678-687.
10. Huang R, Wu H, Yang L. Investigation on condensable particulate matter emission characteristics in wet ammonia-based desulfurization system. J. Environ. Sci. 2020; 92: 95-105.
11. Mao F-F, Zhou Y, Zhu W, Sang X-Y, Li Z-M, Tao D-J. Synthesis of guanidinium-based poly(ionic liquids) with nonporosity for highly efficient $SO_2$ capture from flue gas. Ind. Eng. Chem. Res. 2021; 60: 5984-5991.
12. Zhang Z, Yang B, Ma H. Aliphatic amine decorating metal–organic framework for durable $SO_2$ capture from flue gas. Sep. Purif. Technol. 2021; 259: 118164-118172.
13. Martinez-Ahumada E, Diaz-Ramirez ML, Velasquez-Hernandez MdJ, Jancik V, Ibarra IA. Capture of toxic gases in MOFs: $SO_2$, $H_2S$, $NH_3$ and $NO_x$. Chem. Sci. 2021; 12: 6772-6799.
14. Chen F, Lai D, Guo L, Wang J, Zhang P, Wu K, Zhang Z, Yang Q, Yang Y, Chen B, Ren Q, Bao Z. Deep desulfurization with record $SO_2$ adsorption on the metal–organic frameworks. J. Am. Chem. Soc. 2021; 143: 9040-9047.
15. Savage M, Cheng Y, Easun TL, Eyley JE, Argent SP, Warren MR, Lewis W, Murray C, Tang CC, Frogley MD, Cinque G, Sun J, Rudić S, Murden RT, Benham MJ, Fitch AN, Blake AJ, Ramirez-Cuesta AJ, Yang S, Schröder M. Selective adsorption of sulfur dioxide in a robust metal–organic framework material. Adv. Mater. 2016; 28: 8705-8711.
16. Brandt P, Nuhnen A, Lange M, Möllmer J, Weingart O, Janiak C. Metal–organic frameworks with potential application for $SO_2$ separation and flue gas desulfurization. ACS Appl. Mater. Inter. 2019; 11: 17350-17358.
17. Brandt P, Xing S-H, Liang J, Kurt G, Nuhnen A, Weingart O, Janiak C. Zirconium and aluminum MOFs for low-Pressure $SO_2$adsorption and potential separation: Elucidating the effect of small pores and $NH_2$ groups. ACS Appl. Mater. Inter. 2021; 13: 29137-29149.
18. Suo X, Yu Y, Qian S, Zhou L, Cui X, Xing H. Tailoring the pore size and chemistry of ionic ultramicroporous polymers for trace sulfur dioxide capture with high capacity and selectivity. Angew. Chem., Int. Ed. 2021; 60: 6986-6991.
19. Cui X, Yang Q, Yang L, Krishna R, Zhang Z, Bao Z, Wu H, Ren Q, Zhou W, Chen B, Xing H. Ultrahigh and selective $SO_2$ uptake in inorganic anion-pillared hybrid porous materials. Adv. Mater. 2017; 29: 1606929-1606937.
20. Carter JH, Han X, Moreau FY, da Silva I, Nevin A, Godfrey HGW, Tang CC, Yang S, Schröder M. Exceptional adsorption and binding of sulfur dioxide in a robust zirconium-based metal–organic framework. J. Am. Chem. Soc. 2018; 140: 15564-15567.
21. Mondal A, Balasubramanian S. Understanding $SO_2$ capture by ionic liquids. The Journal of Physical Chemistry B 2016; 120: 4457-4466.
22. Gao S, Zhang P, Wang Z, Cui G, Qiu J, Wang J. Ionic liquid functionalized 3D mesoporous FDU-12 foreffective $SO_2$capture. ACS Sustainable Chem. Eng. 2020; 8: 586-593.
23. Zeeshan M, Nozari V, Yagci M B, Isık T, Unal U, Ortalan V, Keskin S, Uzun A. Core-shell type ionic liquid/metal organic framework composite: an exceptionally high $CO_2/CH_4$ selectivity. J. Am. Chem. Soc. 2018; 140: 10113-10116.
24. Han G, Liu C, Yang Q, Liu D, Zhong C. Construction of stable IL@MOF composite with multiple adsorption sites for efficient ammonia capture from dry and humid conditions. Chem. Eng. J. 2020; 401: 126106-126112.
25. Han G, Yu N, Liu D, Yu G, Chen X, Zhong C. Stepped enhancement of CO2 adsorption and separation in IL-ZIF-IL composites with shell-interlayer-core structure. AIChE J. 2021; 67: 17112-17119.
26. Gu X, Han G, Yang Q, Liu D. Confinement–Unconfinement Transformation of ILs in IL@MOF Composite with Multiple Adsorption Sites for Efficient Water Capture and Release. Adv. Mater. Interfaces

2022; 9: 2102354.

27. Bromberg L, Diao Y, Wu H, Speakman SA, Hatton TA. Chromium(III) terephthalate metal organic framework (MIL-101): HF-free synthesis, structure, polyoxometalate composites, and catalytic properties. Chem. Mater. 2012; 24: 1664-1675.
28. Shin S, Yoo DK, Bae Y-S, Jhung SH. Polyvinylamine-loaded metal–organic framework MIL-101 for effective and selective $CO_2$ adsorption under atmospheric or lower pressure. Chem. Eng. J. 2020; 389: 123429.
29. Ferreira TJ, Ribeiro RPPL, Mota JPB, Rebelo LPN, Esperanca JMSS, Esteves IAAC. Ionic liquid-impregnated metal-organic frameworks for $CO_2/CH_4$ Separation. ACS Appl. Nano Mater. 2019; 2: 7933-7950.
30. Mohamedali M, Ibrahim H, Henni A. Incorporation of acetate-based ionic liquids into a zeolitic imidazolate framework (ZIF-8) as efficient sorbents for carbon dioxide capture. Chem. Eng. J. 2018; 334: 817-828.
31. Ferreira IC, Ferreira TJ, Barbosa AD, de Castro B, Ribeiro RP, Mota JP, Alves VD, Cunha-Silva L, Esteves IA, Neves LA. Cr-based MOF/IL composites as fillers in mixed matrix membranes for $CO_2$ separation. Sep. Purif. Technol. 2021; 276: 119303.
32. Long J, Dai W, Zou M, Li B, Zhang S, Yang L, Mao J, Mao P, Luo S, Luo X. Chemical conversion of $CO_2$ into cyclic carbonates using a versatile and efficient all-in-one catalyst integrated with DABCO ionic liquid and MIL-101(Cr). Microporous Mesoporous Mater. 2021; 318: 111027-111037.
33. Hassan HMA, Betiha MA, Mohamed SK, El-Sharkawy EA, Ahmed EA. Stable and recyclable MIL-101(Cr)–Ionic liquid based hybrid nanomaterials as heterogeneous catalyst. open Journal of Molecular Liquids 2017; 236: 385-394.
34. Xiong J, Zhu W, Li H, Xu Y, Jiang W, Xun S, Liu H, Zhao Z. Immobilized fenton-like ionic liquid: Catalytic performance for oxidative desulfurization. AIChE J. 2013; 59: 4696-4704.
35. Hajipour AR, Heidari Y, Kozehgary G. Silica grafted ammonium salts based on DABCO as heterogeneous catalysts for cyclic carbonate synthesis from carbon dioxide and epoxides. RSC Adv. 2015; 5: 22373-22379.
36. Lee G-Y, Lee J, Vo HT, Kim S, Lee H, Park T. Amine-functionalized covalent organic framework for efficient $SO_2$ capture with high reversibility. Sci. Rep. 2017; 7: 1-10.
37. Yin MJ, Xiong XH, Feng XF, Xu WY, Krishna R, Luo F. A robust cage-based metal–organic framework showing ultrahigh SO2 uptake for efficient removal of trace $SO_2$ from $SO_2/CO_2$ and $SO_2/CO_2/N_2$ mixtures. Inorg. Chem. 2021; 60: 3447-3451.
38. Zhang Y, Chen Z, Liu X, Dong Z, Zhang P, Wang J, Deng Q, Zeng Z, Zhang S, Deng S. Efficient $SO_2$ removal using a microporous metal–organic framework with molecular sieving effect. Ind. Eng. Chem. Res. 2020; 59: 874-882.
39. Zhang Y, Chen Z, Liu X, Dong Z, Zhang P, Wang J, Deng Q, Zeng Z, Zhang S, Deng S. Efficient $SO_2$ removal using a microporous metal-organic framework with molecular sieving effect. Ind. Eng. Chem. Res. 2020; 59: 874-882.
40. Wang A, Fan R, Pi X, Hao S, Zheng X, Yang Y. N-doped porous carbon derived by direct carbonization of metal–organic complexes crystal materials for $SO_2$ adsorption. Cryst. Growth Des. 2019; 19: 1973-1984.
41. Gong W-Q, Wu X-L, Li Z-M, Zhou Y, Zhu W, Tao D-J. Sulfate ionic liquids impregnated 2D boron nitride nanosheets for trace $SO_2$ capture with high capacity and selectivity. Sep. Purif. Technol. 2021; 270: 118824-118830.
42. An X-C, Li Z-M, Zhou Y, Zhu W, Tao D-J. Rapid capture and efficient removal of low-concentration $SO_2$ in simulated flue gas by hypercrosslinked hollow nanotube ionic polymers. Chem. Eng. J. 2020; 394: 124859-124866.
43. Yi H, Wang Z, Liu H, Tang X, Ma D, Zhao S, Zhang B, Gao F, Zuo Y. Adsorption of $SO_2$, NO, and $CO_2$ on activated carbons: Equilibrium and thermodynamics. J. Chem. Eng. Data 2014; 59: 1556-1563.
44. Chen K, Lin W, Yu X, Luo X, Ding F, He X, Li H, Wang C. Designing of anion-functionalized ionic

liquids for efficient capture of $SO_2$ from flue gas. AIChE J. 2015; 61: 2028-2034.
45. Zhao J, Ren S, Hou Y, Zhang K, Wu W. $SO_2$ absorption by carboxylate anion-based task-specific ionic liquids: effect of solvents and mechanism. Ind. Eng. Chem. Res. 2016; 55: 12919-12928.
46. Yang D, Cui G, Lv M. Efficient absorption of $SO_2$ by [Emim][Cl]–[Emim][SCN] ionic liquid mixtures. Energy Fuels 2018; 32: 10796-10800.
47. Li G, Gui C, Dai C, Yu G, Lei Z. Molecular Insights into $SO_2$ Absorption by [EMIM][Cl]-Based Deep Eutectic Solvents. ACS Sustainable Chem. Eng. 2021; 9: 13831-13841.
48. Prasad BR, Senapati S. Explaining the differential solubility of flue gas components in ionic liquids from first-principle calculations. J. Phys. Chem. B 2009; 113: 4739-4743.
49. Firaha DS, Kavalchuk M, Kirchner B. $SO_2$ solvation in the 1-ethyl-3-methylimidazolium thiocyanate ionic liquid by incorporation into the extended cation–anion network. J. solution chem. 2015; 44: 838-849.

**Hosted file**

`image1.emf` available at https://authorea.com/users/501096/articles/581718-a-novel-il-mof-nanocomposite-tailored-for-trace-so2-efficient-capture-based-on-synergistic-effects

**Scheme 1.** Illustration of the preparation of IL/MIL composites.

**Hosted file**

`image2.emf` available at https://authorea.com/users/501096/articles/581718-a-novel-il-mof-nanocomposite-tailored-for-trace-so2-efficient-capture-based-on-synergistic-effects

**Figure 1.** (a) PXRD patterns, (b) $N_2$adsorption/desorption isotherms at 77 K, (c) pore size distribution and (d) FT-IR spectra of IL/MIL-x (0.2, 0.4, 0.7) and MIL-101(Cr).

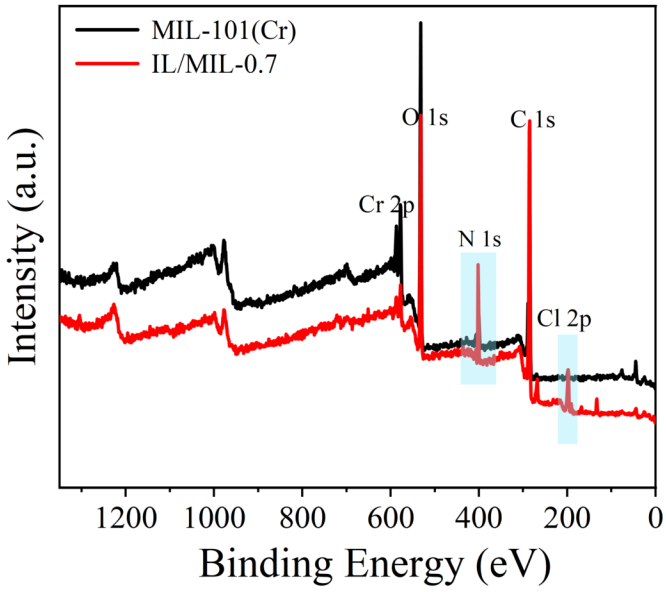


**Figure 2.** XPS spectrum of MIL-101(Cr) and IL/MIL-0.7.

**Hosted file**

image4.emf available at https://authorea.com/users/501096/articles/581718-a-novel-il-mof-nanocomposite-tailored-for-trace-so2-efficient-capture-based-on-synergistic-effects

**Figure 3.** TEM image of IL/MIL-0.7(a) and MIL-101(Cr)(b).

**Hosted file**

image5.emf available at https://authorea.com/users/501096/articles/581718-a-novel-il-mof-nanocomposite-tailored-for-trace-so2-efficient-capture-based-on-synergistic-effects

**Figure 4.** $SO_2$ sorption isotherms for IL/MIL-x (20%, 40%, 70%) and MIL-101(Cr) at 298 K: (a) 0–1 bar. (b) 0–0.1 bar (the desorption isotherms are omitted for clarity in a, b).

**Hosted file**

image6.emf available at https://authorea.com/users/501096/articles/581718-a-novel-il-mof-nanocomposite-tailored-for-trace-so2-efficient-capture-based-on-synergistic-effects

**Figure 5.** (a) $SO_2$, $CO_2$ and $N_2$adsorption isotherms of IL/MIL-0.7 at 298 K; (b) comparison of the $SO_2$ uptake of IL/MIL-0.7 with reported materials (more details in SI).

**Hosted file**

image7.emf available at https://authorea.com/users/501096/articles/581718-a-novel-il-mof-nanocomposite-tailored-for-trace-so2-efficient-capture-based-on-synergistic-effects

**Fig. 6.** IAST selectivity for $SO_2/CO_2$ mixtures (10/90) of IL/MIL-0.7 at 298 K and 1.0 bar (a); and comparison of the separation performance of $SO_2/CO_2$: (b) selectivity at 298 K and 1.0 bar, and (c) $S_{sp}$ at 298 K.

**Hosted file**

image8.emf available at https://authorea.com/users/501096/articles/581718-a-novel-il-mof-nanocomposite-tailored-for-trace-so2-efficient-capture-based-on-synergistic-effects

**Figure 7.** (a)The column breakthrough curves for $SO_2$(2000 ppm)/$CO_2$/$N_2$separation with IL/MIL-0.7 at 298 K and 1 bar; (b) $SO_2/CO_2$ breakthrough selectivity ((1), (3): 2000 ppm/15/84.8, v/v/v, $SO_2/CO_2/N_2$; (2): 5000 ppm/10/89.5, v/v/v, $SO_2/CO_2/N_2$).

**Hosted file**

image9.emf available at https://authorea.com/users/501096/articles/581718-a-novel-il-mof-nanocomposite-tailored-for-trace-so2-efficient-capture-based-on-synergistic-effects

**Figure 8.** (a) $SO_2$ adsorption isotherm at 273 K, 298 K; (b) $CO_2$ adsorption isotherm at 273 K, 298 K; (c) $SO_2$ adsorption heat; and (d) $CO_2$adsorption heat of IL/MIL-0.7.

**Hosted file**

image10.emf available at https://authorea.com/users/501096/articles/581718-a-novel-il-mof-nanocomposite-tailored-for-trace-so2-efficient-capture-based-on-synergistic-effects

**Figure 9.** (a) 4 consecutive adsorption cycles of IL/MIL-0.7; (b) FT-IR spectra of IL/MIL-0.7 after adsorption and desorption; (c) TGA curve of IL/MIL-0.7.

**Table of Contents**

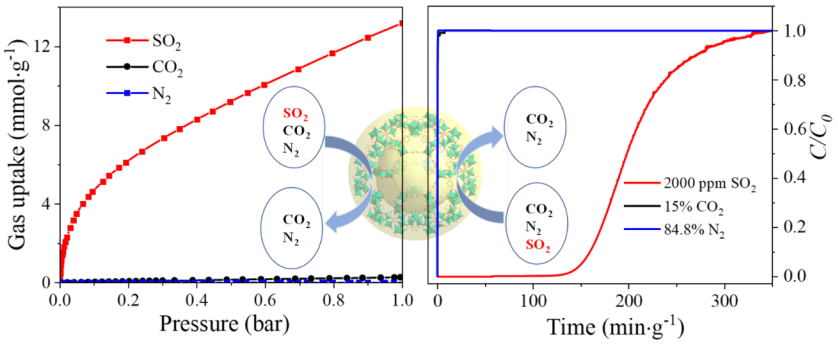


A new type of IL/MOF composite was prepared through a precise design to achieve deep removal of sulfur dioxide ($SO_2$), and the molecular sieving of $SO_2$, $CO_2$, and $N_2$ can be achieved.